Biotechnology Journal
www.biotechnology-journal.com

Scaled-Up Inertial Microfluidics: Retention System for Microcarrier-Based Suspension Cultures

Reza Moloudi, Steve Oh, Chun Yang, Kim Leng Teo, Alan Tin-Lun Lam, Majid Ebrahimi Warkiani, and May Win Naing**

Recently, particle concentration and filtration using inertial microfluidics have drawn attention as an alternative to membrane and centrifugal technologies for industrial applications, where the target particle size varies between 1 µm and 500 µm. Inevitably, the bigger particle size (>50 µm) mandates scaling up the channel cross-section or hydraulic diameter ($D_H > 0.5$ mm). The Dean-coupled inertial focusing dynamics in spiral microchannels is studied broadly; however, the impacts of secondary flow on particle migration in a scaled-up spiral channel is not fully elucidated. The mechanism of particle focusing inside scaled-up rectangular and trapezoidal spiral channels (i.e., 5–10× bigger than conventional microchannels) with an aim to develop a continuous and clog-free microfiltration system for bioprocessing is studied in detail. Herein, a unique focusing based on inflection point without the aid of sheath flow is reported. This new focusing mechanism, observed in the scaled-up channels, out-performs the conventional focusing scenarios in the previously reported trapezoidal and rectangular channels. Finally, as a proof-of-concept, the utility of this device is showcased for the first time as a retention system for a cell–microcarrier (MC) suspension culture.

1. Introduction

Migration of neutrally buoyant particles across the streamline was discovered in a macro-sized channel by Segré and Silberberg in the 1960s.[1] Similarly, an induced hydrodynamic lateral lift force originating from the shear gradient rate[2] was applied in a microchannel, which has found a new field of inertial microfluidics.[3,4] Inertial microfluidics has drawn much attention in many multidisciplinary fields, particularly, applications in which manipulation of cells within bodily fluids is of great importance. The most important features of inertial microfluidic systems are their passive nature and higher throughput[5] as compared to active cell or particle separation methods such as dielectrophoresis, acoustophoresis, etc., making them ideal candidates for translation into practice.

Inertial focusing inside straight microchannels has been utilized extensively such as sheathless flow cytometry,[6] cell separation,[7–9] etc. To achieve higher control of lateral particle equilibrium positions inside a channel, geometry-induced secondary flow has been developed. The interplay between the drag force of secondary flow and the inertial lift force results in differentially size-based equilibrium positions.[10] Among various channel structures that induce secondary flow, e.g., asymmetric,[3] serpentine,[11] contraction/expansion,[12] and curvilinear,[13] spiral microchannels have been applied broadly due to the higher throughput, reliability, and the ability to separate multisized particles simultaneously. The demonstrated working Reynolds number for the operation of spiral microchannels,

$$Re = \rho_f U_{avg} D_H / \mu \quad (1)$$

where ρ_f is the density of the fluid, D_H is the hydraulic diameter of the channel, and μ is the dynamic viscosity of fluid, can reach

R. Moloudi, Prof. C. Yang
School of Mechanical and Aerospace Engineering
Nanyang Technological University (NTU)
50 Nanyang Avenue, Singapore 639798

R. Moloudi, Dr. M. Win Naing
Bio-Manufacturing Programme
Singapore Institute of Manufacturing Technology (SIMTech)
Agency for Science, Technology and Research (A*STAR), Innovis
Singapore 138634
E-mail: winnaingm@SIMTech.a-star.edu.sg

Dr. S. Oh, K. L. Teo, Dr. A. T.-L. Lam
Stem Cell Group
Bioprocessing Technology Institute
Agency for Science, Technology and Research (A*STAR), Centros
Singapore 138668

Dr. M. Ebrahimi Warkiani
School of Biomedical Engineering
Center for Health Technologies
University of Technology Sydney
Ultimo, Sydney NSW, 2007, Australia
E-mail: majid.warkiani@uts.edu.au

Dr. M. Ebrahimi Warkiani
Institute of Molecular Medicine
Sechenov University
Moscow, Russia 119146

DOI: 10.1002/biot.201800674

$Re \approx 400$[14,15] in comparison with other aforementioned structures, which normally range from 50 to 200 ($50 < Re < 200$). In the past decade, numerous applications of spiral inertial microfluidics have been shown that can be mainly categorized into separation, e.g., circulating tumor cells (CTCs) enrichment from patient's peripheral blood[16] and concentration or filtration, such as syringe cell concentrator[17] and removal of blood cells for enhancing recovery of viral nucleic acid.[18] Inertial microfluidics throughput is scaled out relatively easily via multiplexing microchannels due to passive focusing of bioparticles, which is dependent only on hydrodynamic forces. Cell retention devices for perfusion bioreactors at a large scale of 0.5 L min^{-1}[19,20] and high-throughput plasma extraction from diluted bloods[21] with a total flow rate of 24 mL min^{-1} were demonstrated through a massive parallelization of spiral microchannels.

Unlike biological sample processing where the target particle size is of the order of ≈10 µm, inertial focusing has drawn attention recently for other industrial applications, such as water treatment and bioprocessing in which the target particle size is of the order of ≈100 µm.[22] Enlarged particle sizes of ≈10× necessitate scaling up of channel dimensions based on the empirical linear function of $a/D_H > 0.07$ (a is the particle diameter)[3] to maintain inertial focusing and to also avoid clogging channels. Having benefited from scalability along with parallelization, Miller et al.[22] recently demonstrated the concentration and classification of large polystyrene particles with total throughout of ≈1 L min^{-1} by stacking 20 toroidal spiral channels. In this study, to reduce the channel footprint and boost the Dean magnitude, although the channel cross-section was scaled up, the radius of curvature was not scaled up correspondingly based on similarity criteria (see Section 3.1).

From the equation

$$De \propto D_H^{1.5} \tag{2}$$

we can conclude that scaling up dimensions of channel cross-sections (≥5×) amplify the Dean vortices noticeably; however, the impact on the secondary flow and inertial particle focusing dynamics has not yet been investigated fully. In trapezoidal spiral microchannels, a size-dependent equilibrium was formed near the outer wall located at the vortex cores,[15,23] which was capable of trapping a broad range of particles after exceeding a critical flow rate. It was shown experimentally that increasing the slope ($\tan\alpha = (H_{\text{outer wall}} - H_{\text{inner wall}})/W$) from ≈0.06 to 0.13 expedited the particle migration toward the outer wall,[15,23] though the underlying mechanism is not fully elucidated. Concentration, purification, and volume reduction processes[19,24] in various industrial and bioprocessing steps refer to one similar process, i.e., the removal or collection of all particles regardless of size. Unlike micron-scale trapezoidal spiral channels ($D_H \ll 0.5$ mm),[15,23] focusing was not established close to the outer wall for scaled-up and low-slant trapezoidal spiral channels ($\tan\alpha < 0.1$).[25] Here, a trapezoidal spiral with a large slant ($\tan\alpha = 0.2$), therefore, was investigated. In addition, particle focusing near the larger side wall can potentially entrap a broader range of particles ($K = a/H_{min} \geq 0.1$, where H_{min} is the shorter side wall), while it is feasible to reach $K \approx 1$ without clogging the channel; however, rectangular spirals have a limitation on the range of particle clogging ratio ($0.07 < K < 0.5$; **Figure 1**A).[14,15,26]

In contrast, we recently showed separation of microcarriers (MCs) from cell suspensions using a scaled-up spiral channel.[25] The established channel, however, cannot function efficiently as a retention system when cells are attached to MCs for MC-based stirred cultures. The MC culture in perfusion bioreactors results in the formation of a broad range of cell–MC complexes that change dynamically. During culture, the cell–MC complexes can attach to each other and then form larger cell clumps.[27,28] This practically introduces diverse sizes of the cell–MC complex that can vary from a single MC (≈175 µm) to a clump consisting of several MCs (>500 µm). Therefore, devising a scaled-up channel that can focus on a broad particle-size distribution is mandatory. To this end, we have investigated a series of scaled-up rectangular and trapezoidal channels. It was found that the increased channel hydraulic diameter (i.e., channel height and width) beyond a critical threshold will dampen the inertia of flow for a given channel Re number, thereby affecting the inertial focusing (Section 4). For example, to provide enough space for even smaller particle-size distribution from ≈100 µm to ≈400 µm, a rectangular spiral channel with the minimum channel height of ≈1 mm is required ($0.1 \leq K \leq 0.4$) but the channel cannot focus on the ≈175 µm MCs ($K = 0.175$) near the inner wall (Figure S9, Supporting Information), as expected, similar to micron-scale channels.[14,26]

In this work, we studied in detail the impacts of scaling up channel dimensions on the secondary flow and particle focusing dynamics in rectangular and trapezoidal spiral channels. We provided more insight into particle focusing dynamics within different loops (i.e., Dean magnitude) of scaled-up spirals and established a focusing map showing the critical threshold of focusing domain. Accordingly, to further boost the working Dean number (i.e., throughput) and elevate the range of particle clogging ratio (K), a scaled-up trapezoidal spiral with a large slant ($\tan\alpha = 0.2$) was designed (Figure 1). Surprisingly, experimental results showed that the fast inertial focusing of large particles ($K = 0.35$) close to the outer wall at a specific Re and De number ($De \approx 50$, $Re \approx 200$)—due to an altered shear-gradient force field (named recently inflection point focusing)[7]—while particles traveling further downstream caused particle mixing for fixed Re and decreasing Dean numbers. Interestingly, the developed inflection point focusing at the first loop showed that it could deal with comparatively higher particle volume fractions ($V_f \approx 3.4\%$) in contrast to conventional focusing at the vortex cores, which can accommodate low-concentration suspensions ($V_f < 0.4\%$). Therefore, a single-loop trapezoidal spiral was found to be sufficient for separation. We have showcased the utility of this device for continuous cell–MC suspension culture retention, which can be easily parallelized to boost the throughput instead of building large-footprint spiral channels.

2. Experimental Section

2.1. Design and Fabrication

A series of spiral channels having four to six loops for both the rectangular and trapezoidal cross-sections were designed.

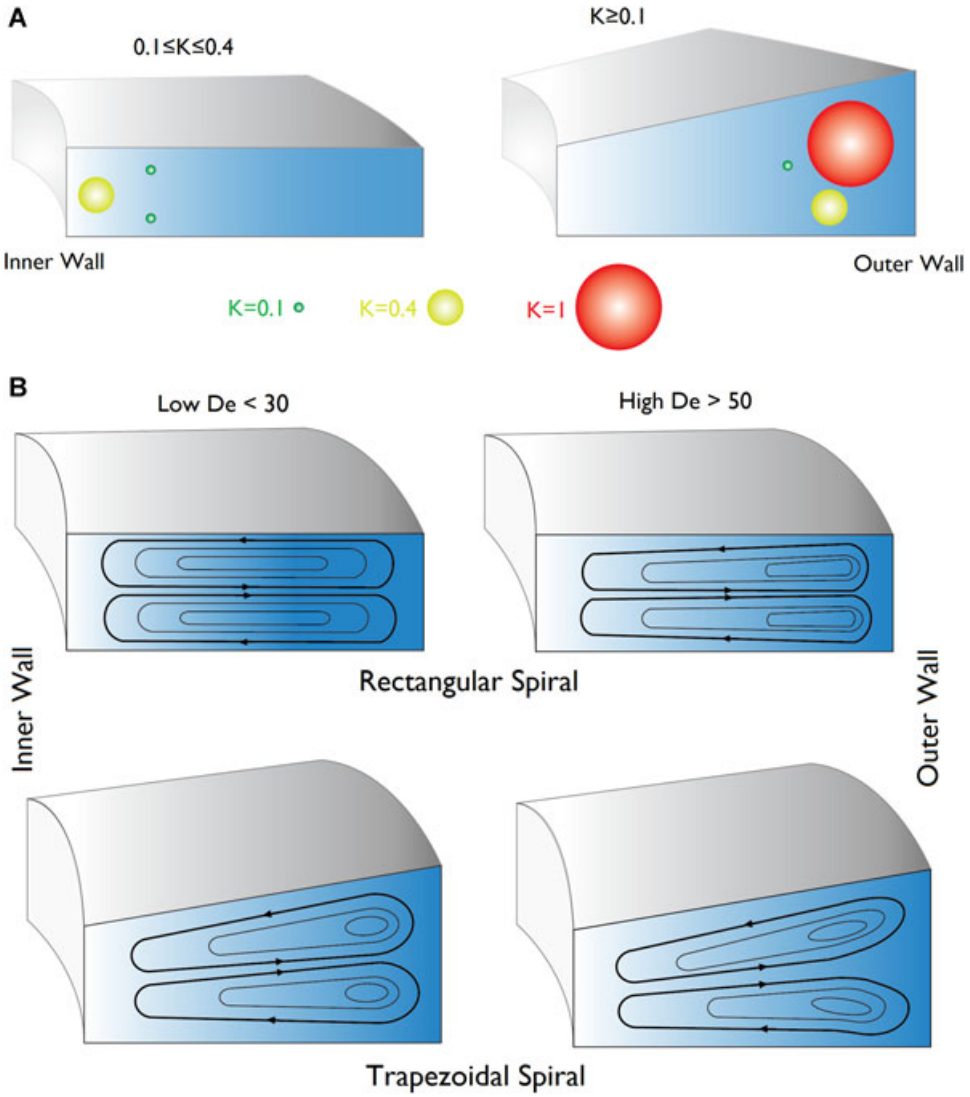

Figure 1. A) Schematic particle equilibriums and variation of the particle clogging ratios (K) in a rectangular spiral and a trapezoidal spiral with a large slant ($H_{\text{outer wall}}/H_{\text{Inner wall}} = 1.8$); a broader particle size distribution can be entrapped close to the outer wall the of trapezoidal spiral. The particle clogging ratio can potentially increase to $K \approx 1$ without clogging the channel. B) Schematic structures of Dean vortices of rectangular and trapezoidal spirals for low and high Dean magnitude. The Dean vortex structure in rectangular spiral channels can be altered by an increase in Dean magnitude itself or a transformation of the cross-section to a trapezoid.

The radius of curvature starts from 5 mm (measured from the inner wall). The minimum channel height $H = 0.5$ mm ($K < 0.5$) was considered to avoid channel clogging (100 µm $< a <$ 250 µm). The moderate channel aspect ratio (AR) of 4 and higher were considered (because the lower AR was not appropriate to have a high-throughput separator device). The heights of rectangular spirals were 0.5 mm and 1 mm, respectively, and the heights of trapezoidal spirals varied between 0.5 mm (inner wall) to 1 mm (outer wall). The width of the spiral channels was 2 mm and 4 mm, respectively. The specifications of all channels are described in Table S1, Supporting Information. The respective MC clogging ratios K and confinement ratios ($C = a/D_H$) are described in the table. The aluminum molds were fabricated using conventional micromilling technique and soft lithography, as described in our previous publication.[25] A 1/16" tubing (Tygon ND-100-65, USA) was used for the inlet and outlet ports.

2.2. Sample Preparation

Different types of neutrally buoyant particles were used to characterize the spiral devices. Fluorescent-labeled particles with 100 µm in diameter (Phosphorex Inc., USA) and 175 µm particles (Cytodex-3, GE Healthcare, USA) were diluted with deionized (DI) water to reach 0.01% and 0.1–0.2% volume fraction, respectively, to decrease particle–particle interaction. To enhance the resolution for bright-field microscopy, Cytodex-3 particles were dyed with trypan blue (0.1% volume fraction).

2.3. Cell Culture

2.3.1. Monolayer Cell Culture

Human bone marrow–derived mesenchymal stem cells (MSCs; RoosterBio, USA) were seeded at 5000 cells cm^{-2} and cultured in T175 flasks (Nunc EasYFlask 175 cm^2 Nuclon Delta Surface, Thermo Scientific, USA) in 40 mL MEM-Alpha (Gibco, USA), supplemented with 10% v/v fetal bovine serum (FBS; Gibco) and 1% v/v penicillin/streptomycin (Pen/Strep; Pen-Strep Solution; Biological Industries, Israel). To perform cell count, 5 µL of Solution 13 stain containing acridine orange and 4′,6-diamidino-2-phenylindole (DAPI; Solution 13 AO-DAPI 1 mL, Chemometec, Denmark) was spiked into 100 µL of the suspended cell sample. The viable cell count was measured using the Nucleocounter (Nucleocounter NC-250; Chemometec).

2.3.2. Stirred Culture

Five grams of Cytodex-3 MC (GE Healthcare) were soaked in 500 mL of 10× Phosphate-Buffered Saline (PBS; 1st Base, Singapore, diluted with DI water in 1:10 ratio) for 3 h, rinsed twice with PBS, and autoclaved. The concentration of the MC stock is 10 mg mL^{-1} of Cytodex-3 in PBS. A 2 mg/mL of Cytodex-3 was seeded with 2.4×10^4cells mL^{-1} cultured in MEM-Alpha, supplemented with 10% v/v FBS and 1% v/v Pen/Strep. A 125 mL disposable spinner flask (Corning, USA) was used. To make up 60 mL of cell–MC culture volume, 12 mL of Cytodex-3 stock solution rinsed with culture medium and 8 mL of cell suspension containing 1.44×10^6 cells were added into 40 mL of culture medium. The spinner flask was agitated at 38 rpm. Cells were cultured on MCs for 7 days in an incubator at 37 °C and 5% CO_2 level. Fifty percent of the fresh culture medium was exchanged for all spinner cultures on days 2, 4, and 6.

2.4. Cell–MC Characterization Assay

2.4.1. Cell Counting

To measure total cell concentration, 100 µL of cell–MC culture was lysed using 50 µL of lysis buffer (Reagent A100 Lysis Buffer; Chemometec), and then 50 µL of stabilizing buffer (Reagent B Stabilizing Buffer; Chemometec) was added and mixed. Five microliters of DAPI (Solution 12; Chemometec) were spiked into the sample. The stained sample (total cells) were counted by the Nucleocounter. To count dead cells, the cell–MC sample was stained with Solution 12 without lysis.

2.4.2. Flow Cytometry

After the cells were harvested, a total of 10^5 cells were resuspended in cold PBS, supplemented with 1% v/v bovine serum albumin (BSA). Cell surface markers CD34, CD90, CD45, CD105, CD73, and CD146 (Biolegend, USA) were analyzed using flow cytometry (Novocyte; ACEA Biosciences Inc., USA). Cells were incubated with the antibodies for 30 min in an ice box and in the dark.

2.5. Numerical Simulations

The spiral channel was simulated using commercial software, ANSYS Fluent. The Hex map mesh was imported from Gambit, and the continuity and Navier–Stokes equations were solved subsequently by using a semi-implicit method for pressure linked equations (SIMPLE) algorithm. The inlet and outlet boundary conditions were set to inlet velocity and ambient pressure. No-slip velocity was applied for walls boundary conditions. Liquid water properties, density of 998.2 kg m^{-3} and dynamic viscosity of 0.001002 kg m^{-1} s^{-1}, were used for fluids. Although much effort has been taken, a comprehensive net inertial lift force model to simulate inertial particle focusing exclusively for spiral channels has not been validated.[29] In this study, flow simulation was only carried out to qualitatively analyze the secondary flow and its impacts on main velocity profile, i.e., inertial lift force.

2.6. Experimental Setup

The fluorescent particle suspension was injected into the spiral channels, mounted on an inverted epifluorescence microscope (Olympus IX71; Olympus Inc., USA) using a syringe pump (F200; Chemyx, USA). The Cytodex-3 suspension was fed by a peristaltic pump (BT300S, LeadFluid). The flow rates varied from 8 mL min^{-1} ($Re \approx 100$) to 24 mL min^{-1} ($Re \approx 300$). To prevent deposition of fluorescent particles, a spherical ball (magnetic stirring bar, polytetrafluoroethylene [PTFE], spherical, 12 mm; Sigma-Aldrich, Singapore) was placed and moved inside the syringe (60 mL BD plastic syringe) intermittently by using another magnetic stirring bar from outside. A magnetic stirrer was used to agitate gently the suspension in the Cytodex-3 inlet reservoir. All channels were first primed by running 70% ethanol for 5 min to clear the residue and air bubbles. The images were taken (16 bits CMOS camera, optiMOS, QImaging) at different loops of the spiral channel ranging from loops 1 to 5. The exposure time was set to 1 s and 100 µs for fluorescent and bright-field microscopy, respectively. One hundred images were staked using ImageJ software to find the location of particle streaks laterally.

3. Results and Discussion

3.1. Particle Focusing Dynamics in the Scaled-Up Trapezoidal Spiral Channel

Figure 2A shows the designed scaled-up trapezoidal spiral (T1) and the corresponding rectangular spiral (R1) compared to a conventional spiral microchannel. The radius of curvature, R, measured from the inner wall, varies considerably from 5 mm (base circle) to 29 mm (loop 6) and the corresponding square root of curvature ratio ($\sqrt{\delta} = \sqrt{De/Re}$) of ≈0.3 and ≈0.1,

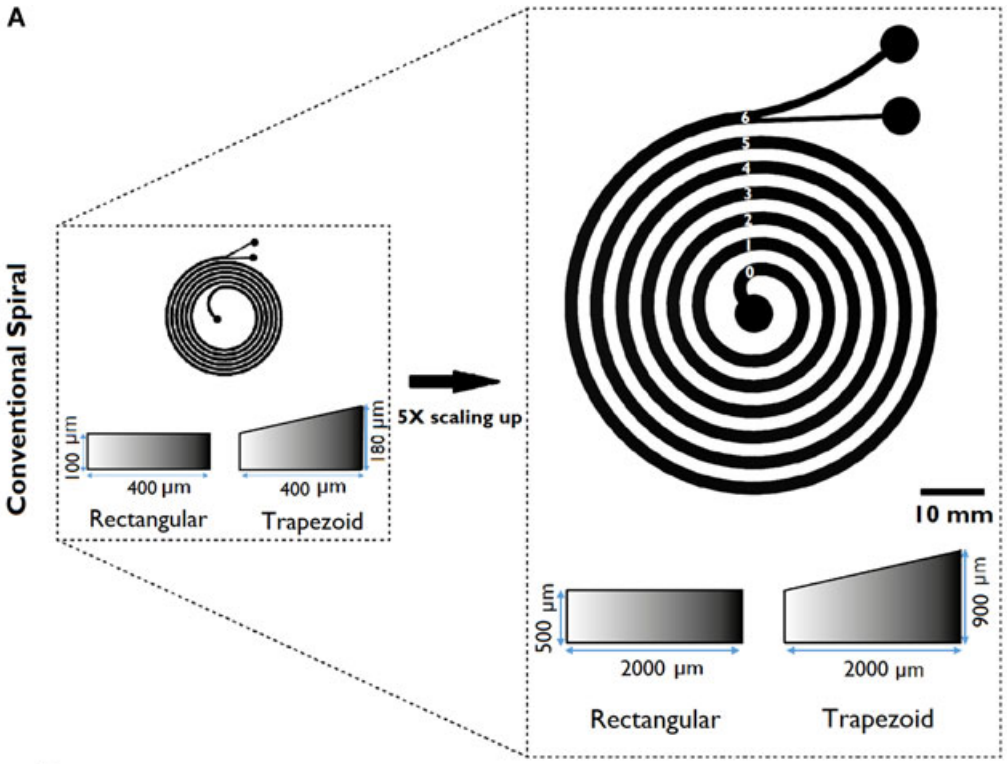

B

Spiral loop	R(mm)	$\sqrt{\delta}$ (Trapezoid)	$\sqrt{\delta}$ (Rectangular)	R(mm) (Conventional Spiral)	$\sqrt{\delta}$ (Conventional Rectangular Spiral)
Base circle	5	0.321	0.283	5	0.126
1st	9	0.239	0.211	5.8	0.117
2nd	13	0.199	0.175	6.6	0.110
3rd	17	0.174	0.153	7.4	0.104
4th	21	0.157	0.138	8.2	0.099
5th	25	0.143	0.126	9	0.094
6th	29	0.133	0.117	9.8	0.090

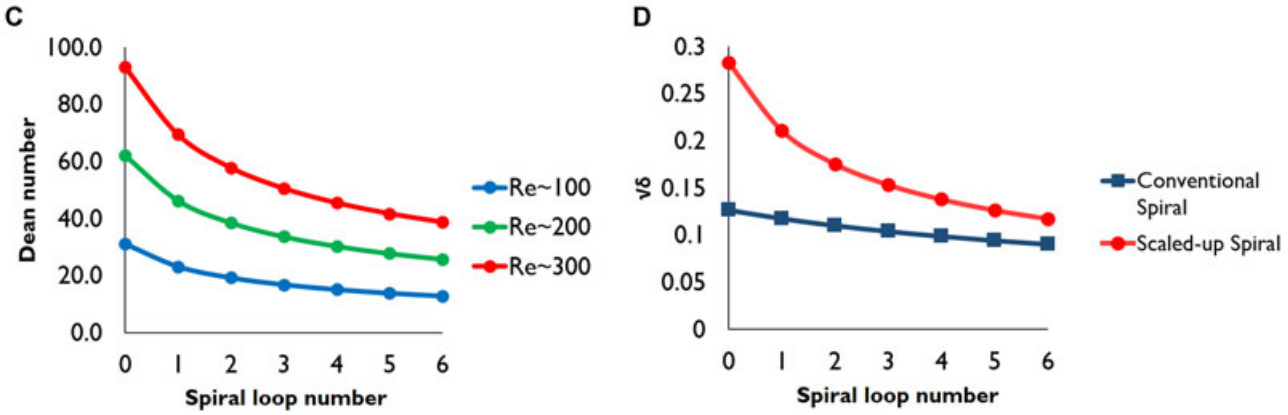

Figure 2. A) Schematic outline of the scaled-up spiral with rectangular and trapezoidal cross-sections compared to a conventional spiral. B) Specifications of curvature ratios for the conventional and the scaled-up spirals. C) Dean profile of the scaled-up spirals for different *Re* numbers. Rapid reduction of Dean magnitude occurs due to significant enlargement of the radius of curvature as a result of scale-up. D) Impact of the scaled-up channel cross-section on curvature ratio ($\sqrt{\delta}$).

respectively (Figure 2B). The radius of curvature of the scaled-up spirals is not enlarged based on similarity criteria to not only reduce the spiral footprint but also increase the Dean magnitude (the scaled-up spirals and the conventional spiral all have a similar radius of curvature at the starting point). The *De* magnitude decreases rapidly at the downstream for a constant *Re* number as shown in Figure 2C. It reduces by 40% from loop 1 to 5, consecutively, when the channel *Re* is constant. To make the impact of scaling up channel cross-section independent of *Re*, the dimensionless parameter of curvature ratio (δ), the ratio of De/Re, is plotted against the conventional spiral (Figure 2D). Scaling up of channel dimensions 5× causes a noticeable increase in the curvature ratio and thus the Dean magnitude. It should be noted that the designed scaled-up spirals cannot be scaled down ≥5× based on similarity criteria due to the restrictions on the innermost radius of curvature; it cannot be reduced to ≤1 mm ($R \leq 1$ mm). To our knowledge, the maximum reported square root of curvature ratio ($\sqrt{\delta}$) for a rectangular spiral channel was ≈0.2 by reduction of the innermost curvature *R* of ≈2 mm.[30]

Figure 3A demonstrates the migration of particles at different loops of the trapezoidal spiral (i.e., various Dean magnitudes) at varying *Re* numbers ($100 \leq Re \leq 300$). At $Re \approx 100$, it is observed that larger particles ($K = 0.35$) mainly migrate toward the outer wall (loop 1) and then slowly sweep back toward the inner wall (loop 5); a clear focusing is not seen. Comparatively, smaller ($K = 0.2$) particles first partially focus next to the outer wall until they reach loop 3. After further travel to the downstream loops, some particles incur secondary drag force and move toward the inner wall while other particles remain trapped at the vortex cores (loop 5). Given that the secondary drag force scales with particle size ($F_D \sim a$), $K = 0.35$ particles are significantly influenced by secondary forces when compared to that effect on $K = 0.2$ particles. Surprisingly, increasing channel *Re* to 200 causes fast migration of $K = 0.35$ particles in loops 1 and 2. Nevertheless, further traveling of particles to the downstream results in particle defocusing and mixing under the influence of the secondary flow. Unlike the larger particles, $K = 0.2$ particles gradually focus perfectly next to the outer wall. Finally, further increasing the *Re* flow to 300 leads to the entrapment of all particles with $K \geq 0.2$ in the vortex cores close to the outer wall (loop 5), as reported previously for the conventional trapezoidal spiral microchannels at high-*Re* flows.[15,23]

The particle movements in the corresponding rectangular spiral are progressively shown in Figure S2, Supporting Information, at different loops as a benchmark. Overall, the moderate magnitude of $Re \leq 200$ can be utilized for particle concentration and filtration where all suspended particles in the mixture with $K \geq 0.2$ mainly focus near the inner wall (loops 4 and 5). Furthermore, one can utilize higher flow rates ($Re \approx 300$) for separation of $K = 0.2$ from $K = 0.35$ particles at a shorter distance (loops 2 and 3), reducing the total spiral footprint.

Figure 3B depicts the evolution of axial velocity profile and structures of Dean vortices by growing the Dean magnitude. Here, to capture the precise structure of Dean vortices, a helicity density (H_d) function is defined numerically (Figure S1, Supporting Information).[31] Helicity density is a pseudoscalar quantity and its variation from positive to negative shows alternating direction of vortex rotation. Figure S3, Supporting Information demonstrates the existence of an inflection point in the axial velocity profile located at the outer half of the channel cross-section for high $De \approx 47$, resulting in fast migration of $K = 0.35$ particles toward the outer wall due to the inflection point focusing in which the direction of shear-gradient lift force switches.[7] Further increasing *De* to ≈70 causes dispersion of $K = 0.35$ particles at loop 1 (Figure 3A, $Re \approx 300$, $K = 0.35$). At high *De* magnitude of ≈70, the core of the maximum axial velocity contour is changed from convex to concave near the outer wall. Investigation of the vortex structure shows that the vortex cores move away from each other, and the boundary of the shear rate in partial axial velocity with respect to height ($\partial V_{axial}/\partial Z$), upon a sign change, alternates along the height and forms a dipole near the outer wall (Figure 3C). Consequently, particles are not able to focus efficiently at loops 1 and 2 (the boundary of the shear rate does not alternate for the rectangular spiral when the Dean magnitude increases to $De \approx 70$, as shown in Figure S4A, Supporting Information. Another major component of the shear-gradient lift force, which could affect the equilibrium state near the inner wall, is the derivative of axial velocity along the channel width ($\partial V_{axial}/\partial y$). Figure S4B, Supporting Information displays a more uniform shear rate field specifically at the inner half of the channel cross-section, i.e., loss of shear-gradient lift force for the trapezoidal spiral).

To elucidate further the observed phenomenon—fast migration of particles to the outer half of the channel cross-section within loop 1 ($Re > 100$, $De > 40$) of the trapezoidal spiral with a large slant, compared to the rectangular spiral—secondary flow is investigated numerically (Figure S5, Supporting Information). Overall, secondary flow dragging particles toward the outer wall at the horizontal midplane reduce for trapezoidal spirals at the inner half of the channel cross-section. Therefore, the main remaining factor responsible for the fast migration of $K = 0.35$ particles (Figure 3A, $Re \approx 200$, loop 1) is the inflection point focusing, which originates from the high *De* magnitude ($De \geq 50$) altering the shear field (Figure S3, Supporting Information).

4. *Re*-D_H Operation Map

Given the well-known influence of particle confinement ratio ($C = a/D_H$) on inertial focusing, a series of scaled-up rectangular and trapezoidal channels were designed systematically to survey the effects of channel hydraulic diameter (D_H) on inertial focusing for large-sized particles (Cytodex-3, $a \approx 175$ µm). All specifications of the channels are described in Table S1, Supporting Information.

The focusing map (**Figure 4**) shows the existence of a critical threshold for the channel hydraulic diameter ($D_H \approx 1$ mm). There is only a narrow zone in which focusing can happen (displayed in green) although, on the basis of theory, a wider range of channel hydraulic diameter ($D_H > 1.6$ mm) is expected for inertial focusing. Scaling up channel hydraulic diameter one order of magnitude from ≈0.1 mm (micron scale) to ≈1 mm (millimeter scale) causes reduction of absolute flow velocity for a given channel *Re* number ($Re \leq 500$). Therefore, the practical ramifications of scaling up is a damping effect on the inertia or

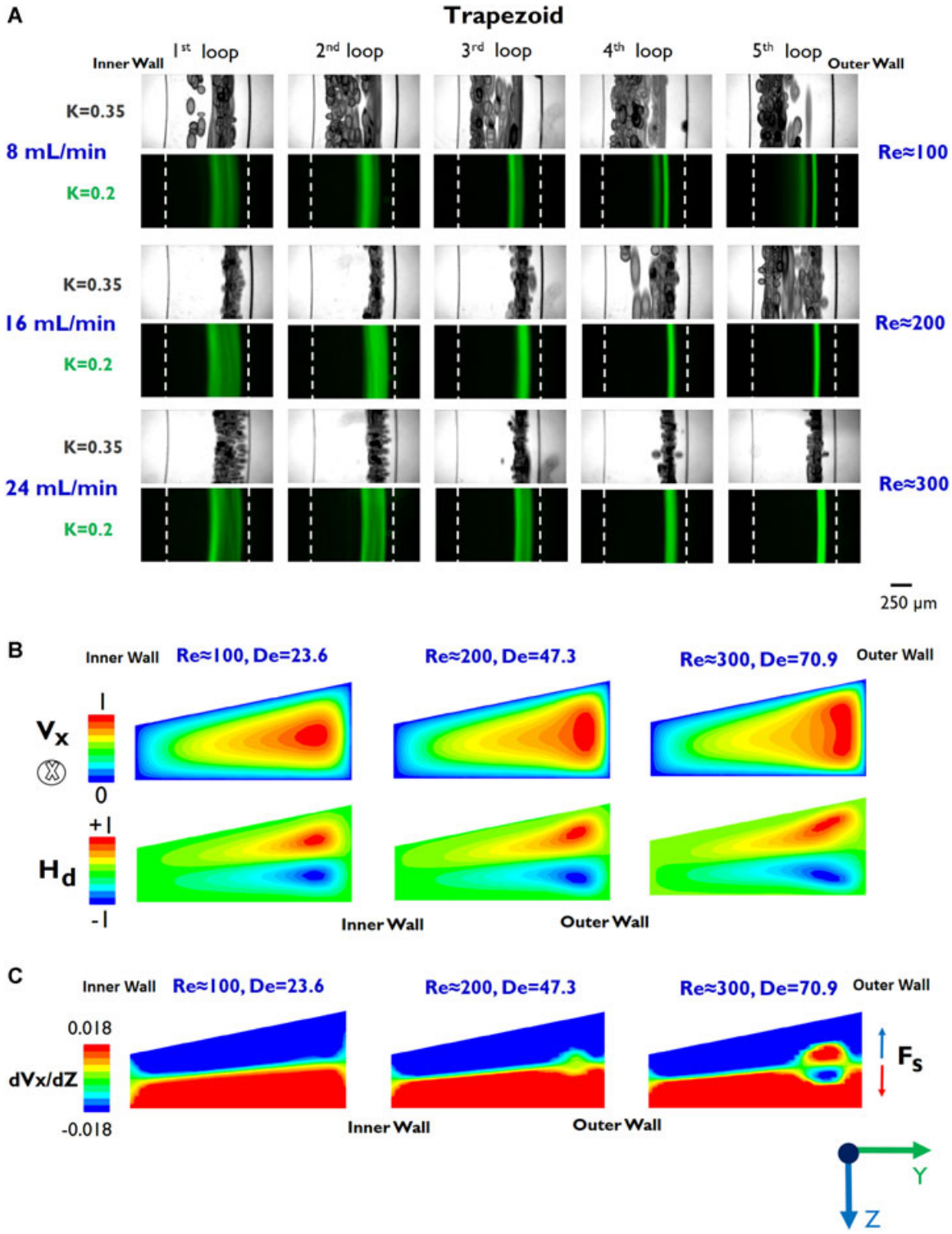

Figure 3. A) Particle focusing of $K = 0.35$ (175 µm, bright field) and $K = 0.2$ (100 µm, fluorescence) at successive loops of the trapezoidal spiral. Interestingly, $K = 0.35$ particles migrate fast toward the outer wall at first loop for $Re \approx 200$ under the dominating shear-gradient lift force while further traveling to the downstream spiral loops causes particle mixing despite the reduction of Dean magnitude by 40%. B) Evolution of dimensionless axial velocity and Dean vortex contour of the trapezoidal spiral by increasing *De* number. C) Dimensionless shear rate field of partial of axial velocity with respect to the height of the trapezoid at the first loop (to find out the boundary where the sign of shear rate alternates, its range is lowered). Increasing Dean to ≈70 results in the formation of a dipole near the outer wall.

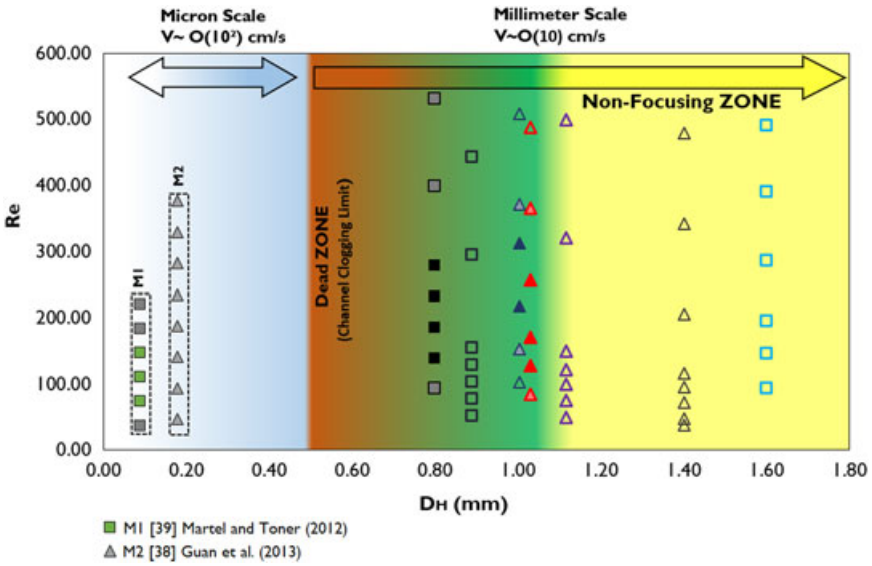

Figure 4. Particle focusing map. The square and triangular markers represent rectangular and trapezoidal channels, respectively. Solid markers show focusing (particle band width $<\approx 4a$), markers with pattern depict partial focusing ($\approx 4a <$ particle band width $< \approx 6a$) and plain markers display nonfocusing (only inside the green zone focusing can be developed for millimeter-scale channels). The focusing map here considers focusing either near the inner wall or the outer wall.

momentum of flow ($U \propto Re/D_H$). Consequently, the secondary flow velocity that is ≈1–10% of average flow velocity is influenced much more severely, resulting in a nonfocusing zone (orange).

Unlike the micron-scale channel, the minimum particle (MC) confinement ratio (C) required is found to be >0.2 and 0.17 for the rectangular and trapezoidal channels, respectively, as shown in Figure S6, Supporting Information (the minimum C reported for a micron-scale particle is >0.07[3]). Accordingly, scaling up channel for larger particle size (250 µm < a < 500 µm) will be more difficult (Figure S7, Supporting Information, $D_H \geq 2$ mm) where the average flow velocity falls below 20 cm s^{-1} even at a large channel $Re \approx 400$ (Figure S8, Supporting Information); therefore, the existence of Dean flow-coupled inertial focusing will be deteriorated.

There are some other factors that can affect inertial focusing at larger particle size ($a \geq 100$ µm). Inherently, possessing a higher coefficient of variation (CV) for large-sized particles (CV > 10%) than that of micron-scale particles (CV < 5%) brings about more restriction in the focusing regime. Finally, the deviation of large-sized particle density from being ideally neutrally buoyant can disrupt inertial focusing further compared to micron-size particle focusing. Scaling gravity force over the inertial lift force ($F_S \sim (U/D_H)^2 a^4$) demonstrates the boosted impact of gravity force for larger channel size as follows:

$$f_g = \frac{mg}{F_S} \sim \frac{\rho_P}{\rho_F} a^{-1} \left(\frac{D_H}{U}\right)^2 \quad (3)$$

where the shear rate $G = U/D_H$ is decreasing for scaled-up channels (reduction of flow velocity and an increase in D_H simultaneously), i.e., the power law function of $1/G^2$ grows faster than canceling the effect of particle size, a^{-1}.

5. MC Concentration and/or Filtration

MC suspensions (≈100 µm to ≈300 µm diameter of beads) are used, along with a stirred tank bioreactor, to increase the culture surface area to volume ratio for scaling up cell culture in cell therapy manufacturing.[28] This is an alternative approach to traditional 2D monolayer cell culture flasks for scaling up anchorage-dependent cell types, such as MSCs. The optimum concentration of MCs has not been reported, as it is dependent on cell type, MC properties, bioreactor type, and culture volume. However, a diverse range of ≈3000 MCs mL^{-1} to ≈15 000 MCs mL^{-1} is reported in the literature.[27,32–40]

Dealing with high particle concentrations is of great importance due to the limits of inertial focusing in low particle volume fractions of <1%,[5,10,15,23] regarded as one of the major drawbacks for many applications. For example, dilution of culture broth in a bioreactor containing MC–cell complexes not only reduces throughput but also imposes some major disadvantages, such as increasing cost of processing and extra concentration step after filtration, which negate the advantages of applying inertial-based (membrane-less) filtration system. To study the effect of particle concentration, four different suspensions with 1500 MCs mL^{-1}, 3000 MCs mL^{-1}, 6000 MCs mL^{-1}, and 12 000 MCs mL^{-1}, corresponding to 0.42%, 0.84%, 1.7%, and 3.4% volume fractions (the ratio of total volume of MCs in unit volume; approximated based on MC concentration and the average diameter of MCs) were prepared.

Figure 5A shows that when the MC volume fraction is equal to 0.42%, the perfect MC focusing for $Re \approx 300$ at the last loop (fifth loop) is spoiled, unlike the low MC concentrations

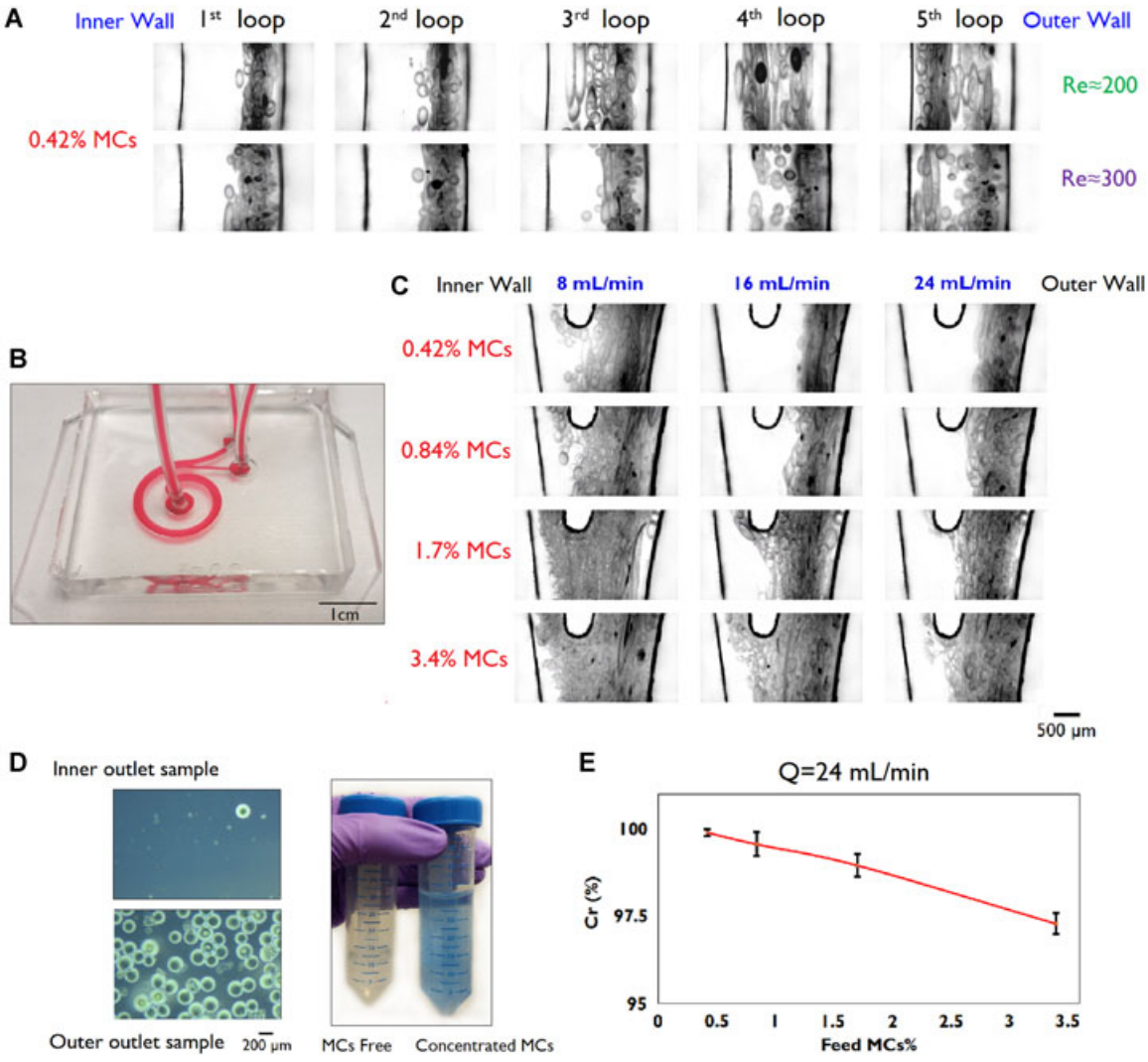

Figure 5. A) Impact of the MC volume fraction of 0.42% on particle focusing at different loops of the trapezoidal spiral for $Re \geq 200$. The particle focusing at fifth loop is ruined even for $Re \approx 300$ when $V_f \geq 0.42\%$, whereas the particle-free region remains at the inner half of the channel cross-section for the first loop. B) Image of the fabricated single-loop trapezoidal spiral channel (the microchannel was filled with a red dye for visualization). C) MC focusing behavior at the bifurcation for different flow regimes and MC volume fractions of 0.42%, 0.84%, 1.7%, and 3.4%. D) Pictures of samples collected from the inner outlet and the outer outlet for 1.7% MCs feed (the concentrated MC sample has a blue color due to the trypan blue-dyed MCs). E) The rejection factor for different MC volume fractions when the flow rate is 24 mL min^{-1} ($n = 3$).

(0.1% MCs, $K = 0.35$, Figure 3A). This particle mixing proves the limitation of inertial focusing, in which the core of Dean vortices exists while excessive number of particles drift to the inner wall and subsequently mix due to the secondary flow drag though its magnitude gradually decreases. Nevertheless, an MC-free zone can be observed next to the inner wall of the first loop regardless of high MC concentration (Figure S10, Supporting Information, $V_f > 0.42\%$), showing the superiority of the inflection point focusing. Therefore, a single-loop spiral channel, which is identical to the first loop of the trapezoidal spiral, along with bifurcation is fabricated to filter and/or concentrate MCs (Figure 5B).

Characterization of the single-loop spiral channel is displayed in Figure 5C for different MC volume fractions. As can be seen for MC suspensions with volume fractions of <1%, a lower flow rate of 16 mL min^{-1} can generate enough shear force to push MCs toward the outer wall (Figure 5C, 0.42% MCs and 0.84% MCs), but increasing the MC volume fraction to >1% results in a wider MC dispersion, which necessitates an increase in the flow rate to ≥24 mL min^{-1} (Figure 5C, 1.7% MCs and 3.4% MCs) to separate MCs efficiently from the outer outlet.

To evaluate the quantity of MCs that are elutriated from the inner outlet, the relative rejection factor (C_r) parameter is defined as follows:[21]

$$C_r = 1 - \frac{C_c}{C_s} \tag{4}$$

where C_c and C_s are the number of MCs collected from MC-free sample (inner outlet) and feed MC in unit volume. The higher

rejection factor represents a lower magnitude of MC loss as well as higher purity in the MC-free sample. Figure 5D shows images of samples collected from the inner outlet (MC-free) and the outer outlet (concentrated MC) for 1.7% MC feed at a flow rate of 24 mL min^{-1}. It should be noted that the ratio of sample volumes collected from the inner to outer outlets is 1:3 because the bifurcation is located about one-third of the channel's width from the inner wall. However, the present single-loop spiral can accept the higher concentration without compromising the purity of the particle-free sample. As demonstrated (Figure 5E), the rejection factor remains almost constant while the increasing MC volume fraction to 1.7% and 3.4% resulting in only ≈1% (n = 3) and ≈2.7% (n = 3) drop in C_r, respectively. The device performance (C_r) for MCs is comparable with the recent large-scale cell retention device's efficiency of ≈99% when the input cell concentration is <≈15×10^6 cells mL^{-1} (V_f ≈ 4.5%).[20]

The proposed single-loop trapezoidal spiral with a large slant, in addition to substantially lesser footprint than that of the

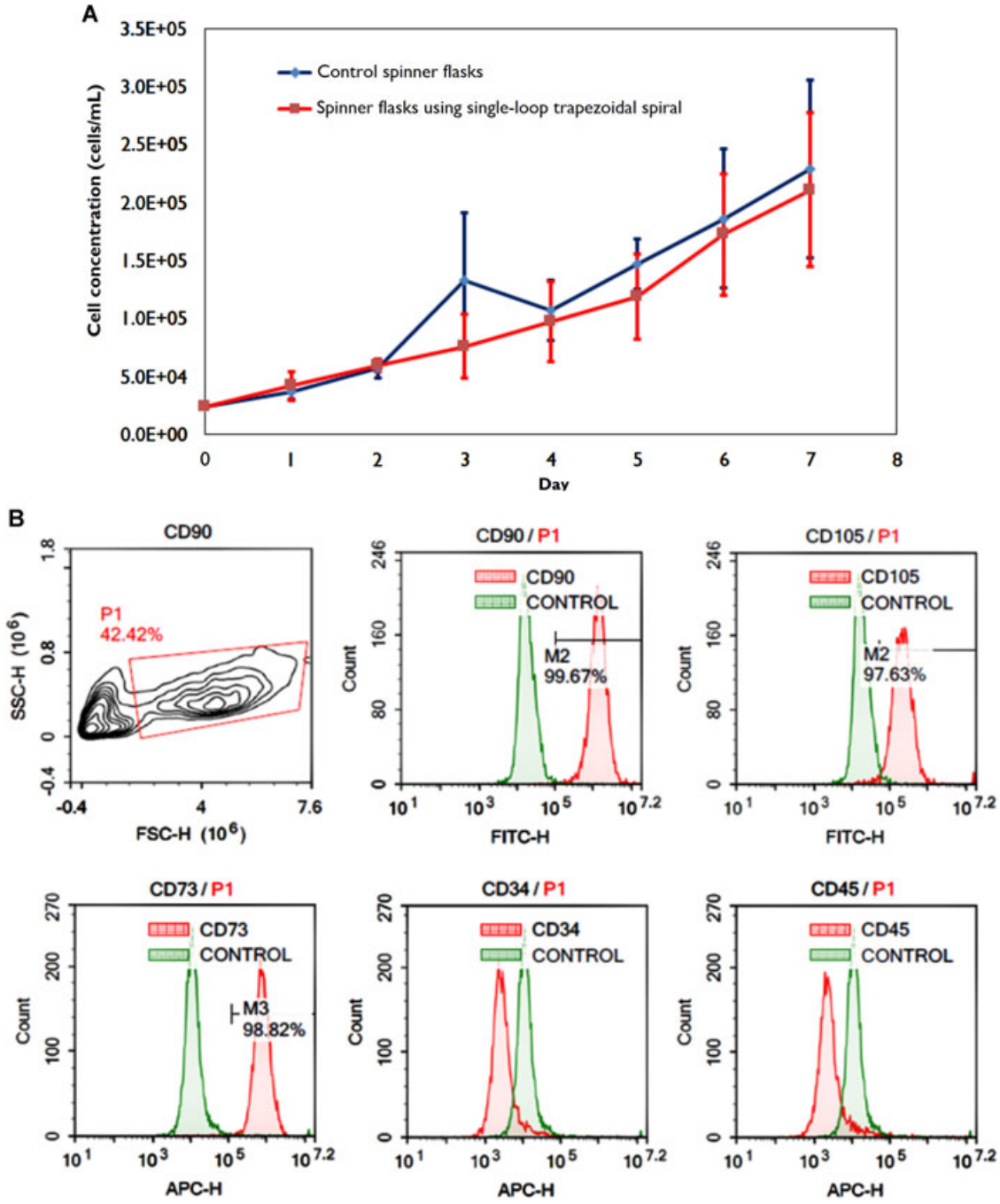

Figure 6. A) Seven-day cell growth profile of human bone marrow–derived MSCs cultured on Cytodex-3 MCs in spinner flasks (n = 3). B) Histograms of cell surface marker expressions harvested at day 7 using the single-loop trapezoidal spiral.

scaled-up spiral with six loops (Figure S11, Supporting Information), can accommodate a broader range of particle clogging ratios ($0.086 < K < 1$) simultaneously due to the large slant (large outer wall). However, in a scaled-up rectangular spiral, the K factor cannot exceed 0.5 due to channel clogging ($0.175 < K < 0.5$). Figure S9, Supporting Information shows no focusing developed for $K = 0.175$ particles in a scaled-up rectangular spiral. An increase in the slant of a trapezoidal spiral will lead to an increase in the hydraulic diameter of channel cross-sections ($D_H > 1$ mm), and thus the minimum cutoff particle size will shift to a larger size. For example, a single-loop trapezoidal spiral with $\tan\alpha = 0.4$ ($H_{\text{outer wall}}/H_{\text{inner wall}} = 2.6$, $H_{\text{inner wall}} = 0.5$ mm, $W = 2$ mm) cannot filter efficiently the MC suspension with $K = 0.35$, i.e., the rejection factor C_r will decrease noticeably (data are not shown).

Finally, among other configurations of trapezoidal spirals applied for particle filtration, the performance of a scaled-up trapezoidal spiral with the larger inner wall was examined (Figure S12, Supporting Information). The results show that its performance is reliant on the low-Re flow of ≈100 regardless of large spiral footprint and low particle volume fraction ($V_f <$ 1%).[18,21] The best focusing is developed adjacent to the inner wall when the Re number is ≈100. An increase in Re results in a wider particle band even for a dilute MC suspension with the low particle volume fraction of ≈0.1%.

6. MC-Based Suspension Culture Retention System

Since cell–MC stirred culture are prone to cell damage due to exposure to high shear rate, two sets of three spinner cultures ($n = 3$) were set up as a case model (described in Section 2.3). The single-loop trapezoidal spiral channel functioned as MSCs–MCs retention system to either harvest conditioned medium or carry out medium change for the spinner cultures. Separated MSC–MC complex from the outer wall outlet was recycled to the spinner flasks (Figure S13, Supporting Information, displays the experiment configuration). Following extraction of conditioned medium from the inner wall outlet using the single-loop spiral (at an inlet flow rate of ≈20 mL min^{-1}, ≈8 min), the fresh medium was added on days 2, 4, and 6.

Although there was ≈1–2% MSC–MC loss from the inner wall outlet, cell culture growth profile (**Figure 6**A) revealed approximately eightfold cell expansion having a similar trend to control spinner flask cultures ($n = 3$). From day 3, clumping of MCs was observed in all sets (Figure S14, Supporting Information). MSCs harvested at day 7 maintained their immunophenotypic expression according to International Society for Cellular Therapy (ISCT) criteria,[41] being positive for CD73, CD90, CD105, and negative for markers CD34 and CD45 (Figure 6B). This suggested that passing the cell–MC complex through the single-loop trapezoidal spiral channel had no adverse impact on cell growth and identity.

We have observed qualitatively smaller MSC–MC clumps, compared to control spinner flask cultures, when using the single-loop spiral channel for a longer period (at day 7, running for ≈20 min). This potentially can be of interest for large-scale bioreactors because smaller clump size makes separation and harvesting of cells easier at the end of cell expansion. Moreover, incorporation of the proposed device into perfusion bioreactors culturing cell–MC is of great interest while running it continuously, which has relative merits compared to some conventional retention systems, such as spin filters, hollow fiber membranes, and centrifugations that are bulky systems suffering from cost of operation and maintenance, membrane replacement, complicated handling, etc. The proposed system can be scaled out relatively easily by multiplexing channels[19–21] due to its passive structure, and we envision that the working MC volume fraction can be further enhanced to be adopted in industrial applications.

7. Conclusion

In this study, the impacts of scaling up channels on Dean flow and subsequent particle focusing in spiral channels with rectangular and trapezoidal cross-sections were investigated in detail. A "focusing map" was established that can be used as a foundation for the design of new microfluidic systems. Unlike the micron scale, the minimum particle confinement ratio ($C = a/D_H$) required was found to be $C \geq 0.2$ and $C \geq 0.17$ for rectangular and trapezoidal channels, respectively, showing notably stringent limitation on the C ratio (the minimum C reported for a micron-scale particle is >0.07). Scaling up channel hydraulic diameter one order of magnitude from ≈0.1 mm (micron scale) to ≈1 mm (millimeter scale) quenches the inertia of flow for a given channel Re number ($Re \leq 500$); as a result, the existence of Dean-coupled inertial focusing is deteriorated ($D_H >$ ≈1 mm).

Moreover, a unique focusing based on inflection point without the aid of sheath flow was explored in the scaled-up trapezoidal channel with a large slant ($\tan\alpha = 0.2$, $D_H \approx 1$ mm). Accordingly, a single-loop trapezoidal spiral was proposed for particle filtration or concentration. Investigation of particle volume fraction demonstrated that the capacity of conventional focusing adjacent to the outer wall in trapezoidal spirals was limited to dilute suspensions with low particle volume fraction ($V_f < 0.42\%$). Regardless, the single-loop trapezoidal spiral with considerably lesser footprint and higher throughput ($Re \geq 200$) showed remarkable performance, based on inflection point focusing, concerning high particle volume fractions ($V_f \approx 3.4\%$) and a broad range of particle clogging ratio ($0.086 < K < 1$). We have showcased the utility of this device as a high-throughput and continuous retention system for stem cell–MC suspension culture. Similar cell expansion trend to control spinners (approximately eightfold expansion) was observed while keeping MSCs' identity.

Supporting Information

Supporting Information is available from the Wiley Online Library or from the author.

Acknowledgements

R.M. would like to thank the SINGA scholarship sponsorship by A*STAR graduate academy, Singapore. This work was supported by Singapore Institute of Manufacturing Technology A*STAR Grant U18-B-017SU

SIMT/18-410006. M.E.W. would like to acknowledge the support of the Australian Research Council via Discovery Project Grant (DP170103704).

Conflict of Interest

The authors declare no conflict of interest.

Keywords

inertial microfluidics, mesenchymal stem cells, microcarrier, retention systems, scale-up, secondary flow

Received: November 5, 2018
Revised: December 23, 2018
Published online: April 15, 2019

[1] G. Segré, A. Silberberg, *Nature* **1961**, *189*, 209.
[2] E. Asmolov, *J. Fluid Mech.* **1999**, *381*, 63.
[3] D. Di Carlo, D. Irimia, R. G. Tompkins, M. Toner, *Proc. Natl. Acad. Sci. U. S. A.* **2007**, *104*, 18892.
[4] A. A. S. Bhagat, S. S. Kuntaegowdanahalli, I. Papautsky, *Microfluid. Nanofluid.* **2008**, *7*, 217.
[5] J. M. Martel, M. Toner, *Annu. Rev. Biomed. Eng.* **2014**, *16*, 371.
[6] S. C. Hur, H. T. Tse, D. Di Carlo, *Lab Chip* **2010**, *10*, 274.
[7] D. Lee, S. M. Nam, J.-A Kim, D. Di Carlo, W. Lee, *Anal. Chem.* **2018**, *90*, 2902.
[8] J. Zhou, C. Tu, Y. Liang, B. Huang, Y. Fang, X. Liang, I. Papautsky, X. Ye, *Sci. Rep.* **2018**, *8*, 9411.
[9] A. Mach, D. Di Carlo, *Biotechnol. Bioeng.* **2010**, *107*, 302.
[10] H. Amini, W. Lee, D. Di Carlo, *Lab Chip* **2014**, *14*, 2739.
[11] J. Zhang, S. Yan, R. Sluyter, W. Li, G. Alici, N.-T. Nguyen, *Sci. Rep.* **2014**, *4*, 4527.
[12] Z. Wu, Y. Chen, M. Wang, A. J. Chung, *Lab Chip* **2016**, *16*, 532.
[13] A. Özbey, M. Karimzadehkhouei, S. Akgönül, D. Gozuacik, A. Koşar, *Sci. Rep.* **2016**, *6*, 38809.
[14] J. M. Martel, M. Toner, *Sci. Rep.* **2013**, *3*, 3340.
[15] G. Guan, L. Wu, A. A. Bhagat, Z. Li, P. C. Chen, S. Chao, C. J. Ong, J. Han, *Sci. Rep.* **2013**, *3*, 1495.
[16] M. E. Warkiani, G. Guan, K. B. Luan, W. C. Lee, A. A. S. Bhagat, P. Kant Chaudhuri, D. S.-W. Tan, W. T. Lim, S. C. Lee, P. C. Y. Chen, C. T. Lim, J. Han, *Lab Chip* **2014**, *14*, 128.
[17] N. Xiang, X. Shi, Y. Han, Z. Shi, F. Jiang, Z. Ni, *Anal. Chem.* **2018**, *90*, 9515.
[18] K. Choi, H. Ryu, K. J. Siddle, A. Piantadosi, L. Freimark, D. J. Park, P. Sabeti, J. Han, *Anal. Chem.* **2018**, *90*, 4657.
[19] M. E. Warkiani, A. K. P. Tay, G. Guan, J. Han, *Sci. Rep.* **2015**, *5*, 11018.
[20] T. Kwon, H. Prentice, J. De Oliveira, N. Madziva, M. E. Warkiani, J.-F. P. Hamel, J. Han, *Sci. Rep.* **2017**, *7*, 6703.
[21] M. Rafeie, J. Zhang, M. Asadnia, W. Li, M. E. Warkiani, *Lab Chip* **2016**, *16*, 2791.
[22] B. Miller, M. Jimenez, H. Bridle, *Sci. Rep.* **2016**, *6*, 36386.
[23] L. Wu, G. Guan, H. W. Hou, A. A. S. Bhagat, J. Han, *Anal. Chem.* **2012**, *84*, 9324.
[24] J. M. Martel, K. C. Smith, M. Dlamini, K. Pletcher, J. Yang, M. Karabacak, D. A. Haber, R. Kapur, M. Toner, *Sci. Rep.* **2015**, *5*, 11300.
[25] R. Moloudi, S. Oh, C. Yang, K. L. Teo, A. T.-L. Lam, M. E. Warkiani, M. W. Naing, *Sci. Rep.* **2018**, *8*, 12481.
[26] J. M. Martel, M. Toner, *Phys. Fluids* **2012**, *24*, 032001.
[27] A. K.-L. Chen, X. Chen, A. B. H. Choo, S. Reuveny, S. K. W. Oh, *Stem Cell Res.* **2011**, *7*, 97.
[28] A. K.-L. Chen, S. Reuveny, S. K. W. Oh, *Biotechnol. Adv.* **2013**, *31*, 1032.
[29] C. Liu, C. Xue, J. Sun, G. Hu, *Lab Chip* **2016**, *16*, 884.
[30] N. Nivedita, I. Papautsky, *Biomicrofluidics* **2013**, *7*, 054101.
[31] H. K. Moffatt, A. Tsinober, *Annu. Rev. Fluid Mech.* **1992**, *24*, 281.
[32] D. Schop, R. van Dijkhuizen-Radersma, E. Borgart, F. W. Janssen, H. Rozemuller, H. J. Prins, J. D. de Bruijn, *J. Tissue Eng. Regener. Med.* **2010**, *4*, 131.
[33] C. J. Hewitt, K. Lee, A. W. Nienow, R. J. Thomas, M. Smith, C. R. Thomas, *Biotechnol. Lett.* **2011**, *33*, 2325.
[34] Q. A. Rafiq, K. M. Brosnan, K. Coopman, A. W. Nienow, C. J. Hewitt, *Biotechnol. Lett.* **2013**, *35*, 1233.
[35] S. Sart, A. Errachid, Y. J. Schneider, S. N. Agathos, *J. Tissue Eng. Regener. Med.* **2013**, *7*, 537.
[36] J. Hupfeld, I. H. Gorr, C. Schwald, N. Beaucamp, K. Wiechmann, K. Kuentzer, R. Huss, B. Rieger, M. Neubauer, H. Wegmeyer, *Biotechnol. Bioeng.* **2014**, *111*, 2290.
[37] P. Gupta, M. Z. Ismadi, P. J. Verma, A. Fouras, S. Jadhav, J. Bellare, K. Hourigan, *Cytotechnology* **2016**, *68*, 45.
[38] A. W. Nienow, Q. A. Rafiq, K. Coopman, C. J. Hewitt, *Biochem. Eng. J.* **2014**, *85*, 79.
[39] A. L. Rodrigues, C. A. V. Rodrigues, A. R. Gomes, S. F. Vieira, S. M. Badenes, M. M. Diogo, J. M. S. Cabral, *Biotechnol. J.* **2018**, *14*, 1800461.
[40] P. Gupta, L. Geris, F. P. Luyten, I. Papantoniou, *Biotechnol. J.* **2018**, *13*, 1700087.
[41] M. Dominici, K. Le Blanc, I. Mueller, I. Slaper-Cortenbach, F. Marini, D. Krause, R. Deans, A. Keating, D. J. Prockop, E. Horwitz, *Cytotherapy.* **2006**, *8*, 315.

